Accepted Manuscript

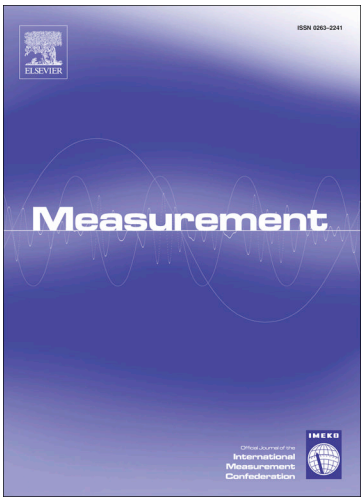

Condition Monitoring of Wind Turbine Pitch Controller: A Maintenance Approach

Asier González- González, Alberto Jimenez Cortadi, Diego Galar, Lorenzo Ciani

PII: S0263-2241(18)30060-5
DOI: https://doi.org/10.1016/j.measurement.2018.01.047
Reference: MEASUR 5222

To appear in: *Measurement*

Received Date: 16 November 2017
Revised Date: 23 January 2018
Accepted Date: 24 January 2018

Please cite this article as: A. González- González, A. Jimenez Cortadi, D. Galar, L. Ciani, Condition Monitoring of Wind Turbine Pitch Controller: A Maintenance Approach, *Measurement* (2018), doi: https://doi.org/10.1016/j.measurement.2018.01.047

This is a PDF file of an unedited manuscript that has been accepted for publication. As a service to our customers we are providing this early version of the manuscript. The manuscript will undergo copyediting, typesetting, and review of the resulting proof before it is published in its final form. Please note that during the production process errors may be discovered which could affect the content, and all legal disclaimers that apply to the journal pertain.

© 2018. This manuscript version is made available under the
CC-BY-NC-ND 4.0 license http://creativecommons.org/licenses/by-nc-nd/4.0/

ACCEPTED MANUSCRIPT

Measurement xx (2018) xx–xx

Contents lists available at ScienceDirect

Measurement

journal homepage: www.elsevier.com/locate/measurement

Condition Monitoring of Wind Turbine Pitch Controller: A Maintenance Approach

Asier González- González[1,*], Alberto Jimenez Cortadi[1], Diego Galar[1,2], Lorenzo Ciani[3]

[1] Tecnalia Research and Innovation, Industry and Transport Division; Miñano (Araba) 01510, Spain, asier.gonzalez@tecnalia.com, alberto.jimenezcortadi@tecnalia.com, diego.galar@tecnalia.com

[2] Luleå University of Technology, Lulea, Sweden, diego.galar@ltu.se

[3] University of Florence, Department of Information Engineering. Via di S. Marta 3. 50139 Florence, Italy, lorenzo.ciani@unifi.it

Article info

Article history:
Received xxxx
Received in revised form xxxx
Accepted xxxxx

Keywords:
Condition Monitoring
Wind turbine
Pitch control
Maintenance

Abstract

With the increase of wind power capacity worldwide, researchers are focusing their attention on the operation and maintenance of wind turbines. A proper pitch controller must be designed to extend the life cycle of a wind turbine's blades and tower. The pitch control system has two main, but conflicting, objectives: to maximize the wind energy captured and converted into electrical energy and to minimize fatigue and mechanical load. Four metrics have been proposed to balance these two objectives. Also, diverse pitch controller strategies are proposed in this paper to evaluate these objectives. This paper proposes a novel metrics approach to achieve the conflicting objectives with a maintenance focus. It uses a 100 kW wind turbine as a case study to simulate the proposed pitch control strategies and evaluate with the metrics proposed. The results are showed in two tables due to two different wind models are used.

1. Introduction

1.1. Wind energy increasing

Renewable energy is growing fast in the world todaybecoming increasingly common, with wind turbines (WT) one of the most popular energy sources. Wind power capacity is increasing exponentially every year around the world; Figure 1 shows the massive increase over the last 40 years.

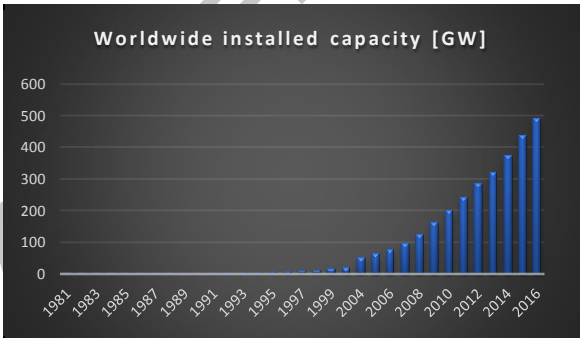

Fig. 1. Accumulative wind power capacity since 1981 (source: GWEC).

According to World Wind Energy Association (WWEA), worldwide wind capacity will reach 540 gigawatts by the end of 2017. The Global Wind Energy Council (GWEC) says the confidence in the wind power market will continue, as the technology is improving, prices are going down, and WTs have a positive impact on climate change by reducing emissions. Figure 2 shows GWEC's forecast of wind power capacity by region between 2017 and 2021.

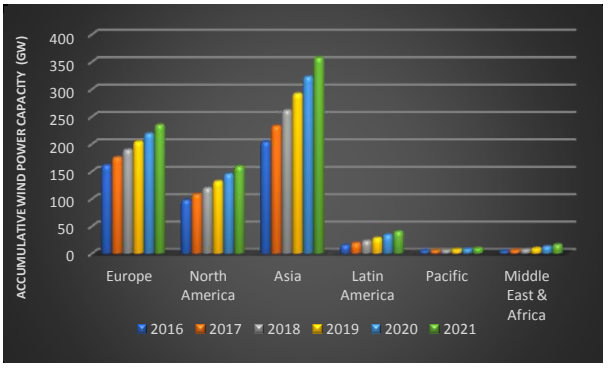

* Corresponding author.
E-mail address: asier.gonzalez@tecnalia.com (Asier Gonzalez-Gonzalez).

ACCEPTED MANUSCRIPT

Fig. 2. Accumulative forecast by region 2017-2021 (source: GWEC).

WTs have evolved from generating a few kilowatts in the 1980s to several megawatts today; this capacity should keep rising in the future. Although the nominal hub rotation speed usually reduces as the WT size increases, the WT power increases approximately by the square of the radius of the expanding WT. Investigations of design limits and solutions for very large wind turbines show that even 20 MW wind turbines are feasible from a technical point of view [1]. The WT unit with one of the largest installed capacities is Vestas V164. These units were first installed in 2016. Figure 3 represents the WT increase in size and power over time.

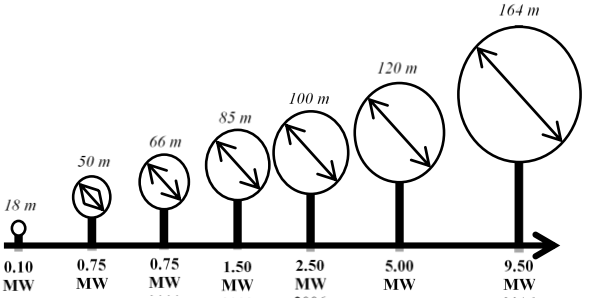

Fig. 3. WT power capacity and size increase over time.

1.2. Wind energy viability

Although the cost of wind energy generation has dropped over recent decades, government support is required for it to be feasible. Excluding subsidies, wind energy projects are economically assessed in terms of the leveled cost of energy (LCOE) [2]. The rate between the entire cost over a WT's lifetime and the amount of energy generated over this lifespan is LCOE, measured as monetary units per energy units, such as €/KWh.

WTs are designed according to the International Electrotechnical Commission (IEC) 61400 series to have almost 20 years of life. Economic costs over that lifetime include: i) installed capital cost (planning, equipment purchase, construction and installation cost) and capital cover (financing fees, return on debt and equity, depreciation, income tax and insurance); ii) component replacement, renovation and retrofit actions; iii) operation and maintenance (O&M) costs; iv) other fees, including land lease, insurance, warrantees and administration.

The net energy production generated over the lifespan is calculated by the WT nominal energy multiplied by several corrective factors: i) capacity factor, i.e., the ratio of the energy produced to continuous maximum energy; ii) availability ratio, i.e., the time for energy generation compared to the entire time in parts per unit; iii) the energy losses in parts per unit, i.e., the losses from the WT machine to the grid and the associated efficiency. The net energy production generated over the lifespan can be calculated by:

$$AEP_{net} = P_r \cdot [CF \cdot (1 - EL) \cdot Av]$$

where P_r is the nominal energy, CF is the capacity factor, Av is the availability time ratio for energy generation and EL is the energy losses, i.e., the loses from the machine to the grid wind farm connection (associated efficiency)

WTs can be on- or offshore installations. Note that the LCOE calculated for onshore projects can fluctuate depending on the geographic location and the WT power capacity. Also, climate change impacts on LCOE due to wind resources will be increased in some regions and decrease in others [3]. Some examples of LCOE values of onshore WT projects are listed following. A 1.5 MW WT machine presented in 2011 a 101.8$ / MWh [2]. Two WT machines with 0.9 and 3.0MW of power respectively presented in 2013 an 87 and 88 USD/MWh correspondingly [4]. A WT project with 1.94 MW per turbine presented in 2015 a $65/MWh [5]. Another WT project with 2.0 MW presented in 2015 a 61$ / MWh [6]. According to the International Renewable Energy Agency (IRENA), the minimum, average and maximum values of LCOE on onshore WTs dropped from 37, 71 and 199 USD/GWh to 24, 56 and 141 USD/GWh respectively during the period 2010-2016.

Some examples of LCOE values of onshore WT projects are listed following. A 3.0 MW WT machine with Offshore Fixed-bottom presented in 2011 a 221.9$ / MWh [2]. A 3.39 MW WT with Offshore Fixed-bottom presented in 2015 a $193 /MWh [5]. A 4.14 MW WT with Fixed-bottom presented in 2015 a 181$ / MWh [6]. A 4.14 MW WT with Floating-bottom presented in 2015 a 229$ / MWh [6]. According to IRENA, the minimum, average and maximum values of LCOE on onshore WTs were reduced from 68, 133 and 227 USD/GWh to 96, 123 and 208 USD/GWh respectively during the period 2010-2016. Although offshore WT projects have certain advantages over onshore projects, for example, less wind turbulence and higher wind speed, offshore projects are less profitable. Furthermore, the LCOE of offshore WT projects depends on the topology of the WT's bottom structure such as whether it is fixed or floating.

Figure 4 compares the LCOE *of different renewable technologies (b*iomass, geothermal, hydropower, solar photovoltaic, solar thermal, onshore wind and offshore wind) for 2010-2016.

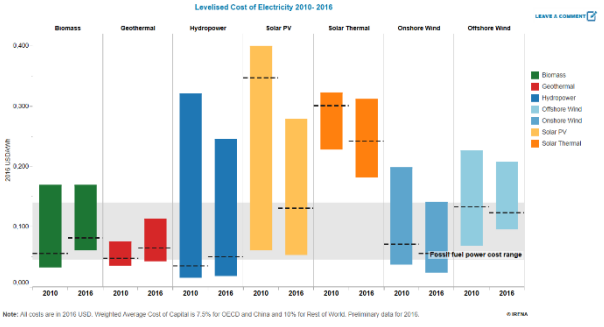

Fig. 4. Levelled cost of energy 2010 – 2016 (source IRENA)

According to the European Commission, strategic targets for offshore wind energy encourage an improvement in the LCOE to less than 100 €/MWh by 2020 and less than 70 €/kWh by 2030.

1.3. Wind turbine size

The size of WTs varies. Each size has its own advantages and disadvantages. Large WTs are generally placed together to produce electricity. These sets of WTs, called wind farms, can be

ACCEPTED MANUSCRIPT

installed on- or offshore. Wind farms share common services and infrastructures with other electrical power types, for example, roads or equipment.

Small and medium sized WT generate less power; the amount of power decreases with the square of the blade radius. In the definition of the International Electrotechnical Commission 61400-2, a small WT stretches a maximum of 200 m2 swept area. This swept area is approximately equal to eight meters of blade radius. According to the Canadian Wind Energy Association (CANWEA), a medium WT generates between one and 300 kilowatts (kW). If WT generates less than 100kW, some authors consider it a small system [7].

Although large WTs have attracted the attention of the manufacturing industry and the scientific community, small and medium sized WTs have several advantages:

Firstly, their visual and environmental impact is less than large WTs because of their reduced size. Small and medium WTs normally use electric current power transmission and do not require special access. In some areas, certain orographic features may prevent the installation of large WTs; their construction may be prohibited or at the very least, an environmental study must be conducted. In contrast, small and medium WTs do not normally require environmental studies before gaining approval.

Secondly, they can be designed for and installed in places with poor wind speed characteristics, for example, discontinuous, turbulent or low wind speeds. The places with best WT characteristics are already occupied, but smaller WTs can be installed in less optimal locations.

Thirdly, installation of small and medium WTs encourages a distributed generation concept and a decentralized electrical energy plan, for example, supplying electricity to a specific community. If one WT fails, the rest continue working.

Finally, smaller WTs can be integrated into urban structures. They can take advantage of existing urban infrastructures, such as access paths. This implies a reduction of direct costs because there is no need to explicitly build and maintain this type of infrastructure. Urban integration also facilitates a short distance between WT energy production and consumption, thus reducing electrical losses due to the Joule effect.

Although it is difficult to calculate the LCOE in Small WTs Due to advantages listed above, a methodology to estimate the LCOE for small and medium WT is presented [7]

1.4. Operation and maintenance (O&M) perspective

1.4.1. Maintenance approaches

From the perspective of O&M, the LCOE can be enhanced by reducing maintenance cost and increasing the availability for energy generation. There are three maintenance approaches. Firstly, reactive or corrective maintenance take place when failures occur during power production time. Secondly, periodic maintenance actions to prevent malfunctions during power production is called preventive maintenance. This maintenance approach is based on time and it normally requires the WT to be idle. Typical maintenance would involve a thorough inspection of the entire system, replacement of fluids, lubrication and servicing of mechanical parts. Thirdly, maintenance actions based on satisfaction certain circumstances are called condition-based maintenance (CBM). This is a continuous process to reveal upcoming faults by monitoring physical parameters. CBM involves certain data analytics process, for example, diagnostics to detect, isolate and identify failures or prognostics to predict failures [8]. The purpose of CBM is to perform maintenance actions at the right time. Figure 5 illustrates the optimum point, i.e., the minimum cost. The use of the correct strategy reduces the entire O&M cost [9]. Also, the effects of maintenance strategies on the life cycle cost of WT can be simulated by bond graphs [10].

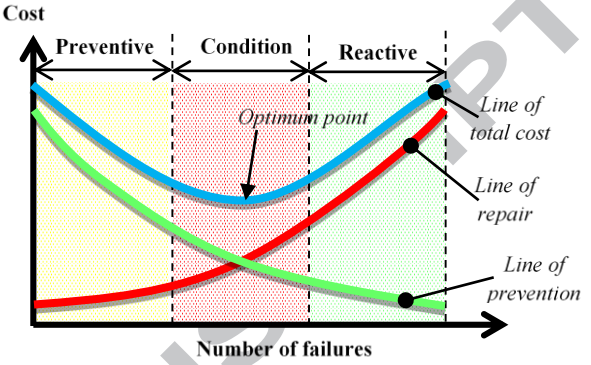

Fig. 5. Costs associated with traditional maintenance strategies.

The non-availability of WTs is mainly caused by three situations. Firstly, certain adverse weather conditions can paralyze the mechanical system. Wind speed below cut-in winds (low wind speed) does not exert enough mechanical energy to generate electrical energy. Alternatively, wind speed above cut-out winds (high wind speed) puts excessive force on WT structures; consequently, WTs are stopped to avoid damage. Secondly, in maintenance operations, the time to perform a repair or replacement generally requires a WT to be in a still state. Thirdly, with component failure, a WT is normally immobile.

However, with the application of efficient maintenance strategies, WT downtime can be greatly reduced. Proper maintenance scheduling uses weather forecast information to plan future preventive actions with the purpose of performing maintenance activities during adverse weather, especially if the WT is likely to be shut down anyway. This strategy increases availability [11].

1.4.2. Wind turbine component failures

Certain WT component failures normally increase with turbine size. Statistical analysis reveals that there are many different factors driving component failure. One is the weather in the location where WT is installed. Although WTs are designed for severe weather conditions, certain extreme events can reduce the components' lifecycle. Wind gusts with extreme wind direction changes at high wind speed can damage structural components, blades or towers for example, as a result of the effect of high aerodynamic forces. Extreme temperatures can have an influence on electronic devices; for example, the calibration of the sensors may be affected. Another factor is the typology of the design, for example, whether the WT has gears or is gearless. An example of the former is a variable-speed direct-drive WT with a full-power AC-DC-AC converter architecture; a shaft connects blades at one end with a generator at the other end. In the latter case, an architecture with a gearbox is commonly constructed with a double feed induction generator. A final consideration is the technology. For example, a focus on

ACCEPTED MANUSCRIPT

pitch system moment requires electric or hydraulic drives. Although the percentage of failures per component require the maintenance times to identify criticality of wind turbine components, figure 6 shows the percentage of failures per component on a WT [9].

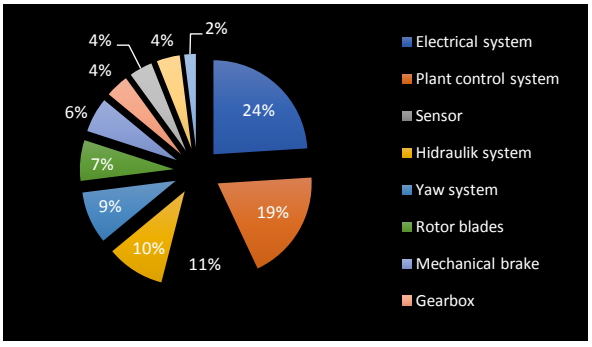

Fig. 6. Percentage of failures per component.

1.4.3. Impact of wind turbine component failure

The economic impact of each component failure is not equal. Failures are critical when they cause downtime or prevent the generation of electricity. Seventy-five percent of the annual WT downtime is caused by only 15% of the failures [12]. Downtime or idle time can be reduced by reducing the frequency of critical failures. The concept of failure mode and effects analysis (FMEA) involves reviewing components and assemblies to identify failure modes as well as their causes and effects. [10]. This increases productivity and reduces the LCOE.

This paper looks at small and medium sized WTs from the perspective of operation and maintenance (O&M). It analyses strategies increase the reliability and availability of WTs. It considers improvements to installed WTs, suggests design possibilities and proposes strategies to extend the WT life cycle.

1.5. Paper organization

The paper is organized as follows. Section 2 gives information on modelling each WT component. Section 3 explains the control systems and methodology used to identify patterns in time series data. Section 4 presents the case study, Section 5 gives simulations and results, and the last section offers conclusions and outlines possible directions for future work.

2. WT as Digital Twin

The digital twin concept refers to an accurate reproduction of a physical wind turbine in a computational system to facilitate understanding and study its behavior. This digital twin representation requires a conceptual model and precise and updated parametrization by gathering data. The purpose of using a digital twin is to reduce downtime and maintenance cost by monitoring and performing diagnostics and prognostics to optimize asset performance and use. The architecture of the proposed digital twin model is shown in Figure 7.

This paper focuses on onshore horizontal axis WTs with variable speed controlled by pitch movement. Although WT modelling requires knowledge from several scientific fields, the proposed model provides a balance of accuracy and computational time [13]. An exhaustive, precise model involves excessive human and computational resources that must be justified [13].

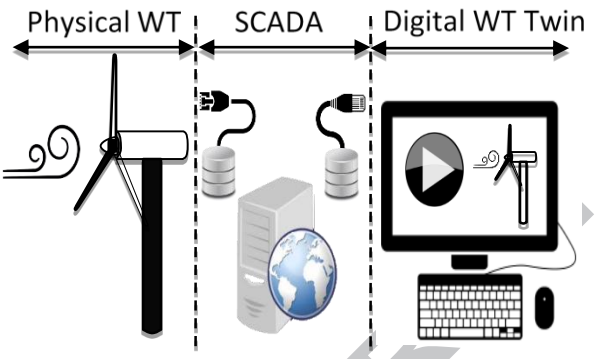

Fig. 7. WT AS DIGITAL TWIN.

Section 2.1 shows diverse wind models used in simulation and methodologies with weather data. Section 2.2 presents aerodynamics concepts used to model the interaction between airflow and WT components exposed to wind. Section 2.3 analyses the behavior of the main structural components and gives information on their materials. Section 2.4 explains the dynamic of the mechanical components. Finally, Section 2.5 explains the interaction between the electric generator (the source), the electric power converter (the conveyance) and the grid (the consumer).

2.1. Wind speed models

Wind is an uncontrollable energy resource, variable in speed and direction over time. Its fluctuations are the main source of disturbances in WT control. It is commonly measured by anemometers and wind vanes. A recent innovation, a LIght Detection And Ranging (LIDAR) system, is able to measure the speed of incoming wind before it reaches a wind turbine rotor [14] [15].

Wind speed characterization at a certain location is normally represented by Weibull distributions [16]. Digital WT-twin simulations require a long chain of consecutive wind speed time series (WSTS) to detect rare events. Infrequent wind speed conditions, such as extreme wind speeds or wind gusts, are modelled and created digitally because it is difficult to gather data on these events. Although there are three-dimensional wind speed models, our simulations do not require such detail. There are many ways to generate WSTS, but they can be divided into deterministic models and random techniques, such as the Monte Carlo method.

2.1.1. Deterministic wind speed time series (WSTS)

2.1.1.1. Wind ramps

A deterministic WSTS is defined easily by a time-dependent function or by multiple sub-functions of the main domain. One example is a wind speed ramp event [17]-[18]. This event is characterized by an increment from lower to higher wind speed. Generally speaking, it is characterized by three parameters: initial wind speed, amplitude and duration of the ramp. It can be defined by a piecewise function as:

ACCEPTED MANUSCRIPT

$$v_{ramp}(t) = \begin{cases} 0 & t < T_{sr} \\ A_{ramp} \cdot \dfrac{(t - T_{sr})}{(T_{er} - T_{sr})} & T_{sr} \le t \le T_{er} \\ A_{ramp} & t > T_{er} \end{cases}$$

where A_{ramp} is the amplitude ramp in [m/s], T_{sr} is the time start ramp in [s], T_{er} is the time end ramp in [s] and t is the time in seconds. Ramp duration is defined as the difference between times T_{er} and T_{sr}. Extreme coherent gust (ECG) is a particular case of a wind speed ramp event defined by the International Electrotechnical Committee (IEC 61400-1) for wind turbine design [19]. Although ECGs have certain predefined values, such as the period of the rise time fixed as 10 seconds and the wind speed increment magnitude defined as 15m/s, other parameters, such as low wind speed, are defined by the wind profile model and hub height [19].

2.1.1.2. Wind gust

An example of a deterministic WSTS is generic wind speed gust. It is defined, in general form, as:

$$v_{gust}(t) = \begin{cases} 0 & t < T_{sg} \\ \dfrac{A_g}{2} \cdot \left[1 - cos\left(2 \cdot \pi \cdot \left(\dfrac{t - T_{sg}}{T_{eg} - T_{sg}}\right)\right)\right] & T_{sg} \le t \le T_{eg} \\ 0 & t > T_{eg} \end{cases}$$

where A_g is the amplitude gust in [m/s], T_{sg} is the time start gust in [s] and T_{eg} is the time end gust in [s].

Extreme operating gust (EOG) is a wind speed gust defined by International Electrotechnical Committee for wind turbine design requirements as a deviation of generic wind gust with a decrement at the beginning and a Mexican hat profile at the end [20].

2.1.2. Wind speed time series information

Several wind speed measurements are available from meteorological stations, often recorded every 10 minutes. For example, Basque Meteorology Agency (Euskalmet) provides minimum, maximum, average and standard deviation of wind speed over a period of 10 minutes. To represent dynamic properties, the ratio between maximum and average wind speed is defined as the gust factor [21]. Atmospheric pressure, humidity and temperature are available every 10 minutes as well. All these data are available on its website. Another example, the Institute for Diversification and Energy Saving (IDAE) offers a Spanish wind atlas on its website. This tool shows the predicted wind potential at a particular location at mesoscale and microscale.

There are many methods to generate artificial WSTS. Hybrid models combining non-parametric and autoregressive models for wind speed forecasting have been suggested [22]. Nested Markov chains have been used to generate long WSTS based on data recorded at two weather stations [23]. A Markov chain method generating WSTS has been compared with a traditional Markov chain method [24]. Other researchers have proposed a method for wind speed forecasting based on determining the representative year's wind speed at a wind farm by interpreting the interaction of the local wind farm and the meteorological station [25]. Another suggested methodology is the simulation of bivariate non-stationary time series of wind speed and direction [26]. Hybrid models consisting of the Empirical Wavelet Transform (EWT), Expectation Propagation (EP) algorithm and Gaussian process regression with the Student-t Observation Model (GPR-t) have been used for short-term wind speed forecasting [27]. Finally, proposed generation model defines four parameters for characterizing the wind speed time series in terms of probability distribution and autocorrelation functions [28].

2.2. Aerodynamic

The interaction between solid objects and air motion is represented by aerodynamic models. Although the main aerodynamic computational effort resides in the blade components, the WT tower also requires an aerodynamic model to simulate dynamic responses.

2.2.1. Blades

2.2.1.1. Advantages and disadvantages of number of blades

The first aerodynamic aspect to consider at the design stage is the number of WT blades. Although a WT designed with three blades is common today, the first WTs had two, as do some recently installed offshore WTs. WTs with three blades have high efficiency, but selecting the number of blades requires choosing between goals:

i) Extra wind power is obtained when a WT blade is added;

ii) Dynamic load fluctuation rises with yawing; this phenomenon decreases with an extra blade;

iii) When the number of blades decreases, the rotation speed is increased to achieve same aerodynamic efficiency, but noise normally increases with speed;

iv) Adding a blade puts an additional burden on the WT structure and requires further design consideration; the extra rotor increases the weight and wind needs extra effort at initial states;

v) Each blade needs an appropriate maintenance routine; more blades mean extra maintenance cost.

Aerodynamic behaviour is characterized by the WT blade shape. The radius of a WT blade is approximately half of the rotor diameter. Figure 8 shows the root, midspan and tip of a WT blade.

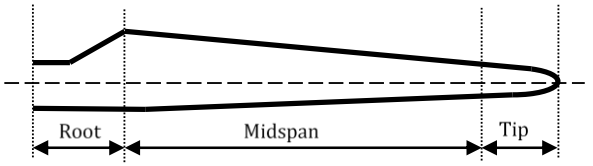

Fig. 8. WT blade.

2.2.1.2. Aerofoil

The cross-sections of a WT blade from the root to the tip are called the aerofoil. Blades normally have different aerofoil profiles at each distance. Figure 9 shows the most characteristic points, segments and lines of an aerofoil.

When the air flows across the aerofoil, this creates lower pressure over the upper convex surface and higher pressure on the lower concave side. This pressure difference is normally represented by two forces, lift and drag, as well as a pitch moment. The angle between chord line and relative wind speed direction is called the angle of attack. These aerodynamic forces fluctuate with changes in the angle of attack.

ACCEPTED MANUSCRIPT

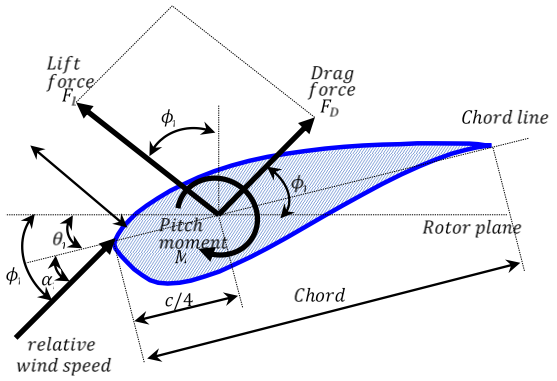

Fig. 9. The most representative aerofoil angles.

2.2.1.3. Fatigue

Because blades rotate around the horizontal shaft, diverse loads are created, the most important of which are air flows, gravity and rotation movement. These loads produce certain undesired effects. The horizontal force exerted by longitudinal wind speed (drag force) produces "flapwise bending" represented in Figure 10. The blades are deflected out of the plane of the rotor towards the wind direction. The blades must withstand these deflections to avoid colliding with the tower itself.

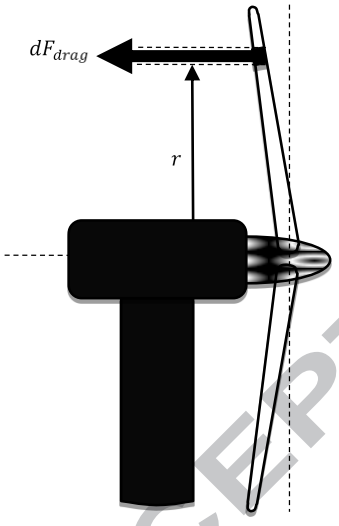

Fig. 10. Flapwise bending.

The gravity and inertial forces produce "edgewise bending" shown in Figure 11. Although these forces are negligible on small blades, they are critical on large blades such as those 70 meters in diameter [29]. Finally, flutter is an instability effect caused by the interaction between the aerodynamic forces and the elasticity of the blade. Flutter leads to rapidly increasing blade vibrations and may ultimately lead to failure.

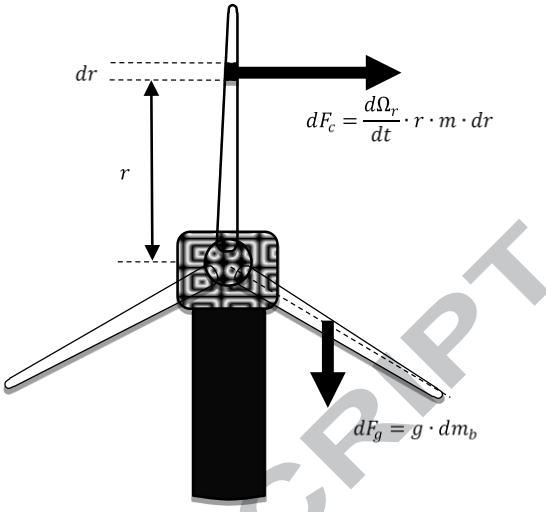

Fig. 11. Edgewise bending

A cyclic loading and unloading in edgewise and flapwise directions cause progressive structural damage to WT blades because of accumulated fatigue damage. These effects can be simulated by aeroelastic models whose advantages and disadvantages are explained in [30]. Using a rainflow-counting algorithm with aerolastic simulations allows individual stress cycles to be identified [31]. Finally, blade lifetime can be estimated using neural network algorithms with existing SCADA signals [32].

2.2.1.4. Aerodynamic power coefficient.

The aerodynamic model is defined by an aerodynamic power coefficient denoted as C_P [20]. When this coefficient is calculated using computational fluid dynamics, the results are accurate. Another technique using assumptions and approximations is blade element theory. The aerodynamic power coefficient is frequently provided as a function of the tip speed ratio λ and the pitch angle β. The tip speed ratio λ is the relationship between tip blade rotational speed and wind speed calculated by:

$$\lambda = \frac{\Omega_r \cdot r_b}{v_1}$$

Figure 12 shows the aerodynamic power coefficient as a function of speed ratio λ and the pitch angle β.

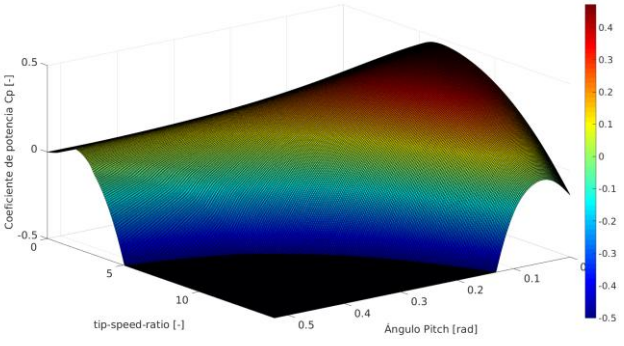

Fig. 12. Aerodynamic power coefficient.

ACCEPTED MANUSCRIPT

Using the aerodynamic power coefficient, the mechanical power extracted by the WT is calculated by:

$$P_r = \frac{1}{2} \cdot \rho_{Air} \cdot r_b \cdot \pi \cdot {v_1}^3 \cdot C_P(\lambda, \beta)$$

Where ρ_{Air} is the air density, v_1 is the wind speed and r_b is the rotor radius. Also, the force that the air exerts on the WT rotor is given by:

$$F_T = \frac{1}{2} \cdot \rho_{Air} \cdot r_b \cdot \pi \cdot {v_1}^2 \cdot C_T(\lambda, \beta)$$

Where $C_T(\lambda, \beta)$ is the thust coefficient. This coefficient is also presented as a function of speed ratio λ and the pitch angle β [2].

2.2.2. Tower

The tower is influenced by the wind as well. A simple model is composed of a wind profile model and an aerodynamic model of the tower. The wind speed profile is calculated by [33]:

$$v(z) = v_{ref} \cdot \left(\frac{z}{z_{ref}}\right)^{\alpha_0}$$

where $v(z)$ is the wind speed at height z, z is the height above groud, α_0 is a wind shear power-law exponent depending on the surface profile and v_{ref} is the reference wind speed at height z_{ref}.

Authors have investigated different tower aerodynamic models, for example, considering aerodynamic damping during the interaction of wind and waves and the structure, and quantitatively evaluating the effects of aerodynamic damping on the lifetime fatigue load on offshore horizontal axis wind turbines towers [34].

2.2. Structural models

Detecting structural damage through periodical observation of dynamic response measurements is called structural health monitoring (SHM). It involves: i) wired sensors connected to a central data acquisition unit via cables, installed during construction of the structure; ii) extraction of damage-sensitive features from sensor measurements; iii) statistical analysis of these features to determine the current state of system health [35].

The most important structural parts are shown in Figure 13 and described below.

Tower is the supporting structure. Normally, it is made of steel, set in a tubular or lattice form. Small WT towers may be made of concrete [36]. Structural response of a hybrid onshore WT tower of lattice structure on the bottom and tubular structure on the top is investigated [37]. The structural response of steel tubular WT tower can be analyzed by Finite Element Method (FEM) [38]. Also, aerodynamic damping and the cross-wind vibrations are investigated on a wind tunnel to determine vortex-shedding correlation lengths and aerodynamic structure coefficients [39].

Hub is the structural component that unites the blades, as well as the pitch bearing is bolted [36]. Also, the hub is fixed to the rotor shaft [36]. The inherent frequencies and vibration modes of Tower, hub and nacelle normally are solved by a modal analysis [40].

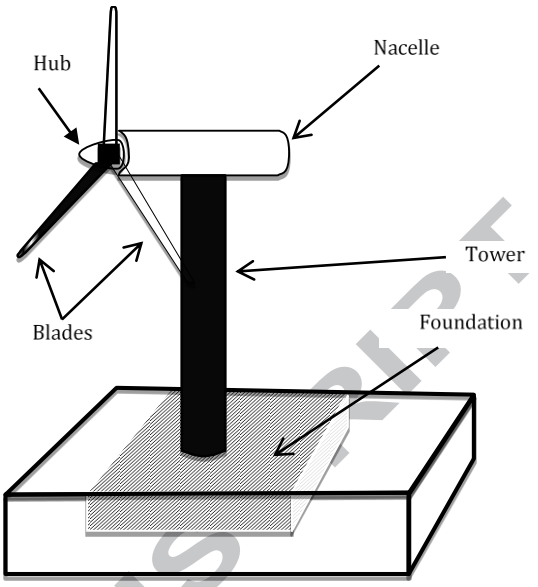

Fig. 13. WT structural components.

Nacelle is the structure housing mechanical and electrical components. The nacelle may be subjected to severe weather conditions that excess technical components specification. To avoid failures caused by extremely high temperatures, an appropriate cooling system is proposed inside the nacelle [41]. The weight and volume reduction of the nacelle can reduce the installation cost as well as the total capital cost [42].

Foundation is designed to transfer the vertical load and to withstand the horizontal dynamic loads caused by the wind. WTs are tall and thin structures, with a high horizontal load variable. The design of the foundations is calculated based on the tipping moment under extreme wind conditions [36]. A comparative study of flat raft, deep flat raft and conical raft foundation solutions is performed [43].

Meteorological unit or "meteorological unit" is the system in charge of monitoring the weather data such as wind speed and direction [44].

Blades: Although aerodynamic blade models were presented in the previous section, a structural model is required to determine the structural dynamic responses. Structural blade models use a 3D FEM, such as ANSYS and Abaqus, or a 1D equivalent beam model [30].

There are several types of blade damage depending on the location:

- Inside the blade: cracks at the bonding resin, missing adhesive, discontinuities on the sandwich, delaminations within the glass fiber reinforced plastics (GFRP) [45] or the sandwich [46], cracks on the web, excess bonding resin [47], problems in the bonding, waves, air inclusions, etc.
- Outside the blade, on the surface: erosion on the blade surface [48], deviations on the laminate (spalling, flaking and cavities), deficient bond at the bonding surfaces [49], cracks [50] and lightning strikes [51, 52]

ACCEPTED MANUSCRIPT

2.3. Mechanical model

The drivetrain is the set of rotating components that transmit the movement from the blades to the electric generator. Their main parts are listed below and shown in Figure 14.

Bedplate is the structure that supports the drivetrain and power generator;

Manin bearing improves slow speed shaft stability by reducing edge loads caused by misalignment errors;

Slow shaft transmits the movement to gearbox; it must endure high torsional stresses;

Gearbox transfers the moment of force from slow speed shaft to high-speed shaft; Gearbox failures are the most common and most critical failure [9]. Historical data show a high failure rate in the gearboxes and they require replacing every five to seven years.

High-speed shaft transfers the moment of force from gearbox to electrical generator;

Brake system is fastened to high-speed shaft; brakes are preserved by hydraulic pressure, but when actuated for safety reasons, the pressure is released and the brake spring presses the assembly against the disc [53].

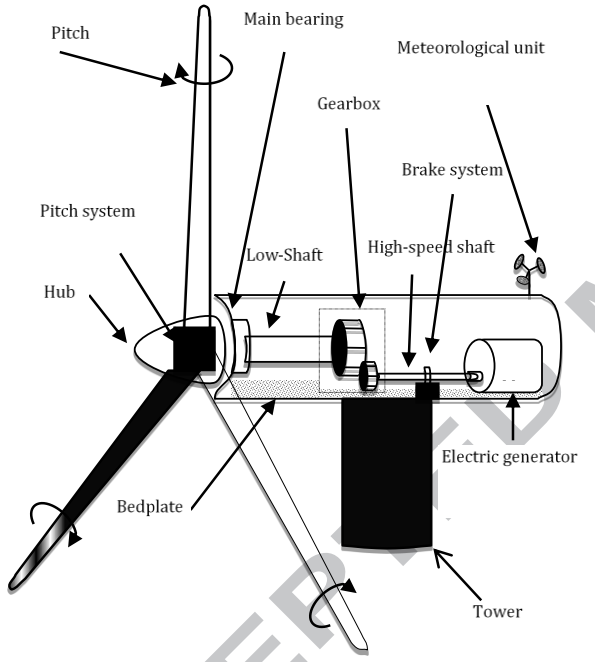

Fig. 14. Main mechanical components.

2.3.1. Drivetrain model

There are different approaches to describe the behaviour of the drivetrain. In general, they are modelled as a set of rigid solids joined by springs and viscous damping with a limited number of degrees of freedom. Some examples are listed following. A drivetrain modelled by two masses joined by torsional rigidity and torsional damping is shown [54]. In [55], the drivetrain consists of 5 parts: rotor, slow shaft, gearbox, quick shaft and generator. A modelling of 5 masses and one equivalent with 2 masses is shown [56]. Two masses are modelled with a torsional damping and a gearbox [57]. The figure 15 shown a proposed model for the drivetrain.

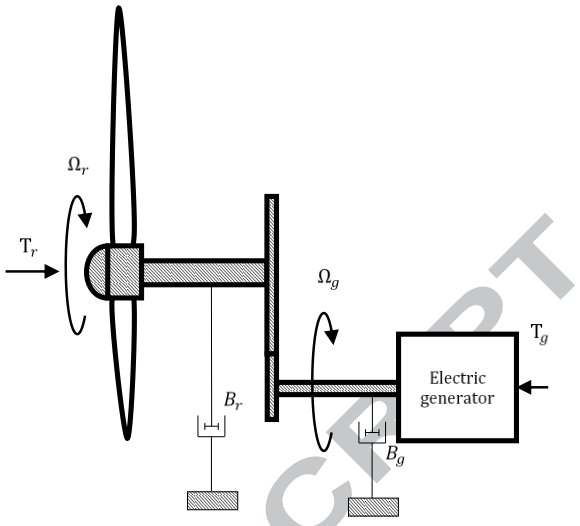

Fig. 15 Pitch angle blade rotation.

Where Ω_r is the rotor angular speed, Ω_g is the generator angular speed, B_r is the damping coefficient of elements at Ω_r (rotor, blade, hub, low-shaft, etc.), B_g is the damping coefficient of elements at Ω_g, I_r moment of inertia of elements at Ω_r ,and finaly, I_g moment of inertia of elements at Ω_g.

2.3.1. Pitch system

Pitch system is a mechanical, electrical or hydraulic device located at the root blade to rotate blades longitudinally in both directions. Figure 14 shows pitch angle WT blade rotation. The pitch speed is proposed to limit by 10 degrees per second in normal operations and 20 degrees per second in emergencies [58]. The pitch angle movement is limited to avoid excessive structural fatigue, it is expressed by

$$\left|\frac{d\beta}{dt}\right| \leq \Delta\beta_{max}$$

Where $\Delta\beta_{max}$ is the maximum pitch speed. The pitch actuator compares the reference pitch angle with the real one. The pitch actuator model is modeled by:

$$\frac{d\beta}{dt} = \frac{1}{\tau_{pa}} \cdot (\beta^* - \beta)$$

Where β is the pitch angle, β^* is the pitch angle setpoint and τ_{pa} is the time constant of pitch drive.

2.3.1. Yaw system

The yaw system**,** shown in Figure 16**,** is in charge of turning the tower to orient the WT towards the direction of the wind. It usually consists of a set of bearings connecting the tower and the nacelle, rotating the nacelle around the vertical axis of the tower, while the tower remains static.

The energy absorbed by the WT decreases due to the misalignment of the rotor axis with the wind direction [59]. The misalignment is measured by diverse techniques[60] [61] [62].

ACCEPTED MANUSCRIPT

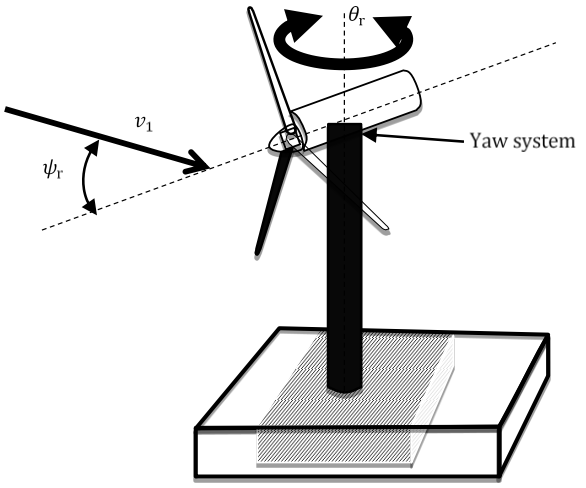

Fig. 16. Yaw system.

The Yaw System can be used to regulate the power absorbed by the rotor when the wind speed is above the nominal speed [63]. It is achieved by reducing the sweep area of the air flow through the rotor plane. The speed of rotation of the Yaw under normal conditions is usually 0.5 grades per second and in cases of emergency, it can rotate 10 grades per second [64].

2.4. Electrical model

The electric model transforms the mechanical energy into electrical energy and pours it into the grid. The electrical system is generally composed of an electric generator and an electric power converter, but there are various types of electrical systems.

i) Squirrel cage induction generator is connected directly to grid. This is a synchronous electrical machine. The WT operates as a constant speed, and electrical torque cannot be controlled. Rotation speed is fixed by grid frequency (normally constant). However, squirrel cage induction generator connected to the grid through a back-to-back converter can control the generator torque [65];

ii) Double-fed induction generator is connected simultaneously to the electric power converter and the grid. The electrical torque is controlled by the electric power converter. Although this generator is a synchronous electrical machine with external excitation, the WT rotation speed is variable [66].

iii) Direct-drive synchronous generator is connected simply to an electric power converter and then to the grid. Electric torque is normally controlled by an AC-DC-AC converter [67].

A sample electrical system with double-fed induction generator typology is shown in Figure 17.

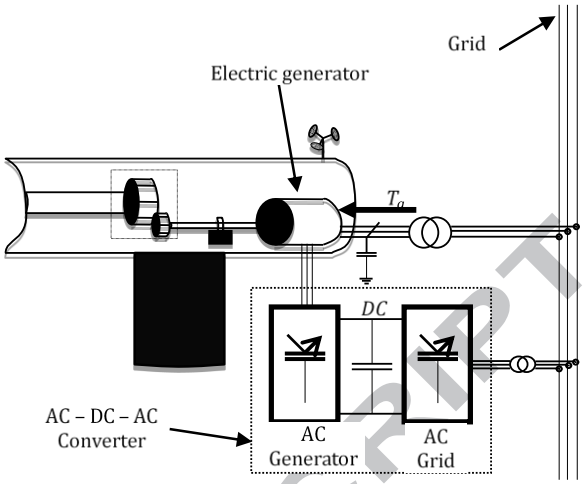

Fig. 17. WT electrical system

The electric generator and converter are modelled by an ordinary differential equation, expressed as:

$$\frac{dT_g}{dt} = \frac{1}{\tau_{ps}} \cdot \left(T_g^* - T_g\right)$$

where T_g^* is the electrical torque setpoint, T_g is the current electrical torque and τ_{ps} is the electric power converter time constant.

3. Control strategies

3.1. Availability, reliability, maintainability, safety, integrity

Pitch controllers are designed to do the following [68]:

- They ensure high **availability** during long periods of operation, e.g., months.
- They guarantee **reliability** under harsh operating conditions, e.g., rain, snow or extreme wind speeds.
- They ensure precise **maintainability** to minimize WT downtime and maximize components' life cycles.
- They ensure **safety** to users and the environment, protecting them from non-desirable outcomes, e.g., electrical generator failure.
- They ensure **integrity**, e.g., such as WT blade fissure.

Availability, reliability, maintainability safety and integrity are targeted so that the failure rate over the life cycle of the components can be reduced. Figure 18 shows one possible theoretical failure rate versus time. This curve represents the bathtub curve where $\beta < 1$ represents a decreasing failure rate, $\beta = 1$ represents a constant failure rate, and $\beta > 1$ represents an increasing failure rate.

ACCEPTED MANUSCRIPT

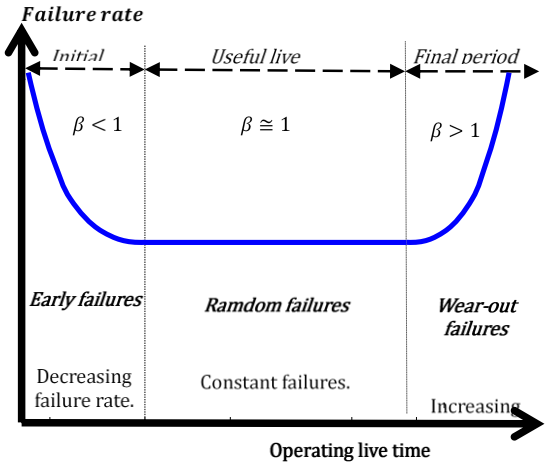

Fig. 18. Failure rate over operating live time.

3.2. Power curve

The electrical power supplied at different wind speeds is generally represented by a power curve graph. Polynomial and exponential curve graphs are the most common [69]. The power curve is given by WT manufacturers and calculated by averaged and normalized measurements [69]. Normally, four regions (I, II, III and IV) and two areas are represented [2]. Figure 19 shows these divisions.

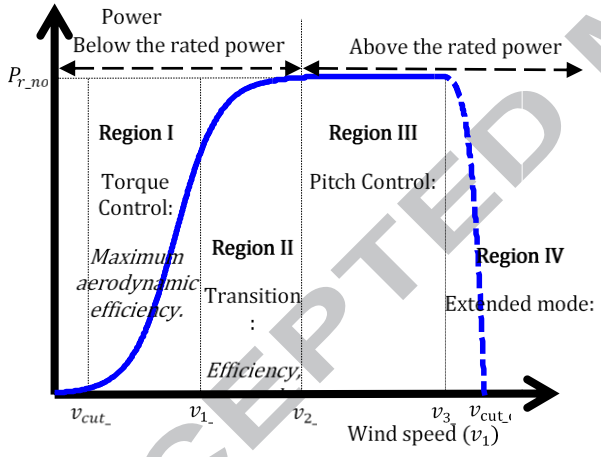

Fig. 19. Power curve.

Region I is the start-up region characterized by low wind speed, from v_{cut-in} to v_{1-2}. Maximum aerodynamic efficiency is achieved by setting the pitch at a minimum angle. Rotor speed is controlled by the demanded electrical torque following wind speed changes.

Region II is the transition region with low and medium wind speed, from v_{1-2} to v_{2-3}. A soft pitch controller is required because the electrical generator controller is the main control in this region.

Region III is the pitch control region characterized by high wind, from v_{2-3} to v_{3-4}. A full pitch controller is required. The demanded electrical torque is proportional to rotor speed.

Region IV is the extended region. In this region, wind speeds are extreme, and the WT is stopped to avoid damage.

3.3. Pitch control

Pitch controller commands pitch drive to move blade pitch angle at certain position to keep rotor speed at a desired setpoint. Typical pitch controller structure is based on a proportional integral control with gain scheduling [70]. Pitch angle setpoint is calculated as:

$$\beta^*(t) = K_P(\beta, \Omega_r) \cdot \left(\Omega_r{}^*(t) - \Omega_r(t)\right) + K_I(\beta, \Omega_r) \cdot \int \left(\Omega_r{}^*(t) - \Omega_r(t)\right) \cdot dt$$

Where β is the pitch angle measured in radians, β^* is the pitch angle setpoint desired, Ω_r is the rotor angular speed in radians per second, $\Omega_r{}^*$ is the rotor angular speed setpoint, K_P is the proportional gain function and K_I is the integral gain function. K_P and K_I are functions of pitch angle and rotor angular speed. Figure 20 shows the control loop scheme of the pitch angle.

Proportional and integral parameters are tuned by analytical methods. Although the transfer function calculation of the closed-loop pitch system involves nonlinear expression due to rotor aerodynamic block is not linear, linear transfer function is achievable by means of Tailor series approximation at rated operation point. The proportional parameter is calculated by:

$$K_P(\beta, \Omega_r) = \left[2 \cdot \xi \cdot \omega_n \cdot I_T \cdot \Omega_{r\_nom} - B_T \cdot \Omega_{r\_nom} + P_{r\_nom} \cdot {\Omega_{r\_nom}}^{-1}\right] \cdot \left[\frac{\partial P_r(\Omega_r, v_1, \beta)}{\partial \beta}\right]^{-1}$$

Where ω_n is the design natural pulsation and ξ is the design damping coefficient. Using a constant rotor speed criteria [20], the integral parameter curve is showed in figure 21.

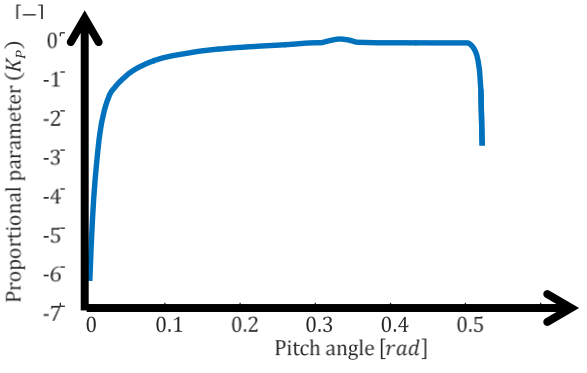

Fig. 21. Proportional parameter curve.

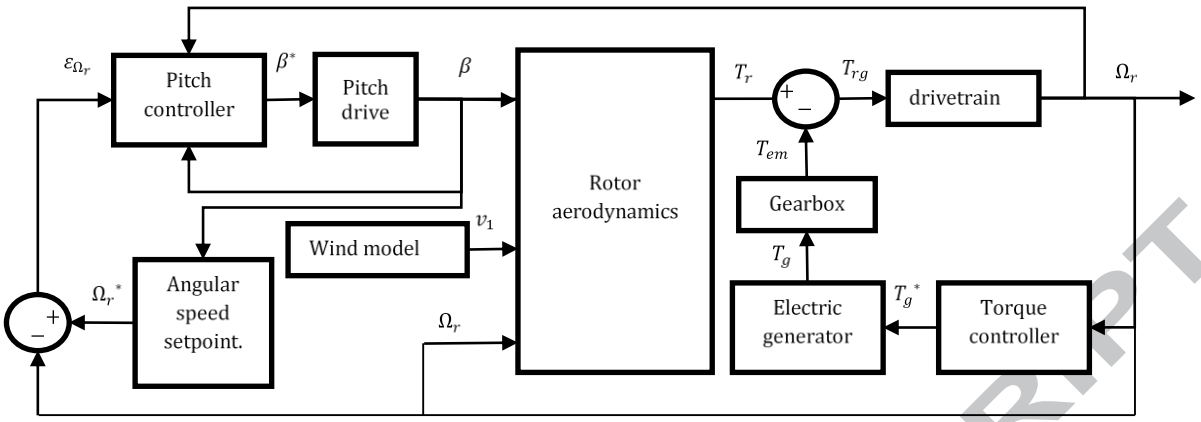

Fig. 20. Scheme for pitch control.

The integral parameter is calculated by:

$$K_I(\beta,\Omega_r) = {\omega_n}^2 \cdot I_T \cdot \Omega_{r\_nom} \cdot \left[\frac{\partial P_r(\Omega_r, v_1, \beta)}{\partial \beta}\right]^{-1}$$

Similarly, using a constant rotor speed criteria [20], the integral parameter curve is showed in figure 22.

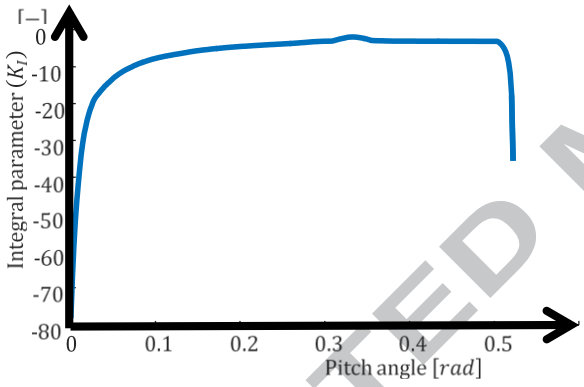

Fig. 22. Integral parameter curve.

There are several strategies to fix the value of rotor speed setpoint. One rotor speed setpoint policy maintains the rotor speed setpoint in a fix value, normally at nominal rotor speed. This constant strategy is analytically defined by:

$${\Omega_r}^* = \Omega_{r\_nom} \cdot (1+\delta)$$

Where δ is the rotor speed setpoint increment or decrement respect of rated speed.

Another strategy, called conventional strategy, increases the rotor speed setpoint proportionally as pitch angle growth. It is analytically defined by a piecewise function as

$${\Omega_r}^*(\beta) = \Omega_{r\_nom} \cdot (1+\delta) + \begin{cases} 0 & \beta < \beta_1 \\ \dfrac{\Delta\Omega_{r\_max}}{\beta_2 - \beta_1} \cdot (\beta - \beta_1) & \beta_1 \le \beta \le \beta_2 \\ \Delta\Omega_{r\_max} & \beta_2 < \beta \end{cases}$$

Where β_1 is the inferior pitch angle, β_2 is the superior pitch angle, Ω_{r_nom} is the nominal rotor speed and $\Delta\Omega_{r\_max}$ is the maximum rotor speed increase. Others mathematical expressions can be used such as exponential or polynomial function.

3.4. Metrics for evaluation

The pitch control system has two main, but conflicting, objectives. On the one hand, it seeks to maximize the wind energy captured and converted into electrical energy. On the other hand, it seeks to minimize fatigue and mechanical load. These objectives are quantified by the metrics proposed below.

The first metric, to maximize the energy delivered to the grid, is represented by:

$$\mathrm{Obj}_1 = \min\left\{-\sum_{t=0}^{t=\infty} |\mathrm{P_r(t)}|\right\}$$

Variations in the rotor angular speed must be avoided because of the possibility of an edgewise bending moment. The WT maintains a constant rotor angular speed, rejecting rotor angular acceleration.

The second metric, to minimize rotor angular acceleration, is represented by:

$$\mathrm{Obj}_2 = \min\left\{\sum_{t=0}^{t=\infty} \left|\frac{\mathrm{d}\Omega_r}{\mathrm{dt}}\right|\right\}$$

Fluctuations in the pitch angle produce aeroelastic forces along the WT blade. Although pitch variations are needed to maintain WT in a precise state during wind speed fluctuation, some over-actuations can occur.

The third metric, to minimize pitch angular speed, is represented by:

$$\mathrm{Obj}_3 = \min\left\{\sum_{t=0}^{t=\infty} \left|\frac{\mathrm{d}\beta}{\mathrm{dt}}\right|\right\}$$

Longitudinal force exerted by the air on the WT rotor must be reduced. To achieve an appropriate efficiency, most wind energy must be transformed by blades into lift force instead of

ACCEPTED MANUSCRIPT

ACCEPTED MANUSCRIPT

drag force (longitudinal force). These longitudinal forces produce a flapwise bending moment on the WT blades.

The fourth metric, to minimize longitudinal force, is given by:

$$\mathrm{Obj}_4 = \min\left\{\sum_{t=0}^{t=\infty} |\mathrm{F_T}(t)|\right\}$$

4. Case study:

The case study WT has 100kW of rate power. Its typology is the horizontal axis. It has three blades with a rotor diameter of 22.5 meters and swept area 471.43 square meters. The tower is 36 meters high and is made of tubular steel. Figure 21 is a picture of the case study WT. Table 1 shows the most representative parameters of aerodynamic model.

Table 1: Parameters of aerodynamic model.

Aerodynamic model	
Parameter	**Value**
$\boldsymbol{\rho_{Air}}$	1.225 [m/s]
$\boldsymbol{P_{r\_nom}}$	100000 [W]
$\boldsymbol{\Omega_{r\_nom}}$	5.23 [rad/s]
$\boldsymbol{r_b}$	11.25 [m]
$\boldsymbol{C_P(\lambda,\beta)}$	Lookup table [-]

Fig. 21. Case study Turbec100Kw. (Courtesy of Argolabe SL)

The control power is regulated by variable speed-pitch control. The wind speed interval production generation begins with cut-in wind speeds at $v_{cut\_in} = 3.5$ m/s and ends with cut-out wind speed at $v_{cut\_off} = 20$ m/s . The power curve is shown in Figure 22. Table 2 shows some parameters of pitch system.

Table 2: Parameters of pitch system.

Pitch system	
Parameter	**Value**
$\boldsymbol{\tau_{pa}}$	0.1 [s^-1]
$\boldsymbol{\Delta\beta_{max}}$	0.17 [rad/s]
$\boldsymbol{\omega_n}$	10 [-]
$\boldsymbol{\xi}$	0.9 [-]

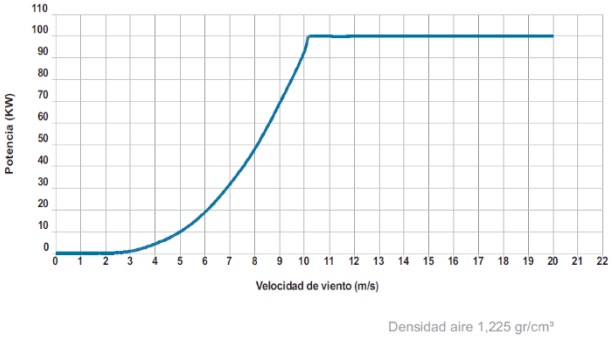

Fig. 22. Power curve of WT case study

The powertrain has a gearbox multiplier with two stages. The specified gearbox transmission ratio is 1:16:9. The electric generator is an 8-pole asynchronous induction generator. The electrical converter is IGBT – total conversion with an output voltage and frequency of 400 V and 50 Hz, respectively. Table 3 shows some parameters of drivetrain model.

Table 3: Parameters of drivetrain model.

Drivetrain model	
Parameter	**Value**
$\boldsymbol{I_r}$	28781 [Kg/m^2]
$\boldsymbol{I_g}$	5.4 [Kg/m^2]
$\boldsymbol{\tau_{ps}}$	8.04 [s^-1]

4.1. Simulations

Several simulations are performed combining various wind speed models, different approaches of controllers and diverse strategies to tuning the rotor speed setpoint. Although there is a wide diversity of wind events suitable to simulate, ramp wind model and wind gust model described on sections before are selected due to wind speed fluctuation is presented in both models. The parameters used for wind models are listed in the table 1.

Table 4: Parameters of wind models.

Ramp wind model		Wind gust model	
Parameter	**Value**	**Parameter**	**Value**
$\mathbf{A_{ramp}}$	15 m/s	A_g	17 m/s
$\mathbf{T_{sr}}$	20 s	T_{sg}	10 s
$\mathbf{T_{er}}$	150 s	T_{eg}	180 s

Although several speed setpoint strategy approaches are assessed, only constant strategy with values around rotor nominal speed are presented. Table 5 and Table 6 show results obtained with ramp wind model and gust wind model respectively. Metrics results are shown by percentage of the best to simplify the comparison between the strategies. The best

ACCEPTED MANUSCRIPT

setpoint strategy for each objective is represented by 100 percent number.

Table 5: Results using ramp wind model

Strategy	Wind model	δ	Obj_1(%)	Obj_2(%)	Obj_3(%)	Obj_4(%)
Constant I	Ramp	-0.10	66.52	69.63	64.95	100.00
Constant II	Ramp	-0.08	68.31	80.25	71.84	99.37
Constant III	Ramp	-0.06	70.88	92.16	82.08	97.57
Constant IV	Ramp	-0.04	77.23	100.00	91.04	90.70
Constant V	Ramp	-0.02	84.45	91.39	82.75	82.96
Constant VI	Ramp	0.00	91.00	81.51	75.12	76.16
Constant VII	Ramp	0.02	93.88	75.13	74.08	74.38
Constant VIII	Ramp	0.04	96.80	71.75	74.52	72.51
Constant IX	Ramp	0.06	100.00	68.56	74.97	70.53
Constant X	Ramp	0.08	91.76	98.93	100.00	83.42
Constant XI	Ramp	0.10	91.86	97.55	99.09	84.95

Table 6: Results using gust wind model

Strategy	Wind model	δ	Obj_1(%)	Obj_2(%)	Obj_3(%)	Obj_4(%)
Constant I	Gust	-0.10	66.50	94.10	87.82	100.00
Constant II	Gust	-0.08	68.47	96.88	90.38	98.98
Constant III	Gust	-0.06	71.40	99.66	96.06	96.66
Constant IV	Gust	-0.04	76.06	100.00	98.34	92.00
Constant V	Gust	-0.02	81.33	98.38	100.00	86.64
Constant VI	Gust	0.00	85.50	94.37	98.43	82.77
Constant VII	Gust	0.02	88.96	89.73	96.43	79.94
Constant VIII	Gust	0.04	92.24	85.44	96.03	77.43
Constant IX	Gust	0.06	95.50	81.29	94.60	75.05
Constant X	Gust	0.08	98.40	77.70	93.83	73.17
Constant XI	Gust	0.10	100.00	76.32	94.02	73.11

5. Discussion

Several simulations are performed by Matlab/Simulink software. The complete model of 100kW WT is implemented according to section 2 as well as control strategies shown in section 3. several winds models, including EOG and ECG. The initial condition of WT reminds in a still state with the pitch angle in minimum value and rotor speed in near to zero value.

The four metrics are proposed to assessment different control strategies. These metrics are conflicting objectives with the purpose of achieving an optimal solution. Capture as much power as possible and reduce the load fatigue are the main targets. A framework combining machine learning and search techniques is a right approach to find miscellaneous solutions in the search space [71].

Compare the solutions obtained in multiobjective scenarios in the existence tradeoff conditions is not trivial. Although results can be compared graphically by pareto frontier, choose analytically the precise strategy can be performed by weighted sum method. This method requires previously set the weights to each metric. Normally, weights values are defined by an expert. Also, it requires scale all metrics into the range [0,1].

In simulations performed, rotor speed setpoint and electrical torque applied to the high-speed shaft are the main regulation parameters. To calculate in each situation, the best suitable setpoint parameters, diverse control strategies are implemented. Some of them are based on metaheuristics algorithms to achieve a compromise solution [20]. The results obtained presents better scores on strategies that include metaheuristics algorithms.

6. Conclusions

Operation and maintenance are challenging for WTs, especially as some of the oldest ones have exceeded their design life of 20 to 25 years. The life cycle of some structural components, such as blades or tower, can be extended if a proper pitch controller is designed. The paper proposes suitable aerodynamic, structural, mechanical and electrical models of a 100kW WT and suggests some control strategies for pitch controller simulations.

It proposes four conflicting metrics to assess pitch controller tuning. The goal is to capture as much power as possible and reject fatigue as a result of the undesired mechanical load. The results indicate that the proposed metrics are suitable for these objectives.

Although additional fatigue metrics can be included, future work on the pitch controller should consider more complex techniques, such as reinforcement learning or metaheuristics optimization, to achieve a proper controller parametrization.

7. References

1. N. Ederer, "The right size matters: Investigating the offshore wind turbine market equilibrium," Energy, vol. 68, no. Supplement C, 2014, pp. 910-921; DOI https://doi.org/10.1016/j.energy.2014.02.060.
2. M. Garcia-Sanz and C.H. Houpis, Wind Energy Systems: Control Engineering Design, Taylor & Francis, 2012.

ACCEPTED MANUSCRIPT

3. D. Hdidouan and I. Staffell, "The impact of climate change on the levelised cost of wind energy," Renewable Energy, vol. 101, no. Supplement C, 2017, pp. 575-592; DOI https://doi.org/10.1016/j.renene.2016.09.003.
4. F.B. Ragnarsson, V.G. Oddsson, R. Unnthorsson and B. Hrafnkelsson, "Levelized Cost of Energy Analysis of a Wind Power Generation System at Búrfell in Iceland," Energies, vol. 8, no. 9, 2015; DOI 10.3390/en8099464.
5. L. National Renewable Energy, E. United States. Department of Energy. Office of Energy Efficiency and Renewable and I. United States. Department of Energy. Office of Scientific and Technical, 2014 Cost of Wind Energy Review, United States. Department of Energy. Office of Energy Efficiency and Renewable Energy, 2015.
6. M. Christopher, M.M. Hand, B. Mark, R. Joseph, H. Donna and H. Jonathan, 2015 Cost of Wind Energy Review, 2017.
7. S. Xu, R. Shao, L. Chang and C. Church, "Energy Cost Estimation of Small Wind Power Systems—An Integrated Approach," IEEE Journal of Emerging and Selected Topics in Power Electronics, vol. 3, no. 4, 2015, pp. 945-956.
8. A.K.S. Jardine, D. Lin and D. Banjevic, "A review on machinery diagnostics and prognostics implementing condition-based maintenance," Mechanical Systems and Signal Processing, vol. 20, no. 7, 2006, pp. 1483-1510; DOI https://doi.org/10.1016/j.ymssp.2005.09.012.
9. P. Tchakoua, R. Wamkeue, M. Ouhrouche, F. Slaoui-Hasnaoui, A.T. Tameghe and G. Ekemb, "Wind Turbine Condition Monitoring: State-of-the-Art Review, New Trends, and Future Challenges," Energies, vol. 7, no. 4, 2014; DOI 10.3390/en7042595.
10. D. Chan and J. Mo, "Life Cycle Reliability and Maintenance Analyses of Wind Turbines," Energy Procedia, vol. 110, no. Supplement C, 2017, pp. 328-333; DOI https://doi.org/10.1016/j.egypro.2017.03.148.
11. G. D'Amico, F. Petroni and R.A. Sobolewski, "Maintenance of Wind Turbine Scheduling Based on Output Power Data and Wind Forecast," Advances in Dependability Engineering of Complex Systems: Proceedings of the Twelfth International Conference on Dependability and Complex Systems DepCoS-RELCOMEX, July 2 - 6, 2017, Brunów, Poland, W. Zamojski, J. Mazurkiewicz, J. Sugier, T. Walkowiak and J. Kacprzyk, eds., Springer International Publishing, 2018, pp. 106-117.
12. K. Fischer, F. Besnard and L. Bertling, "Reliability-centered maintenance for wind turbines based on statistical analysis and practical experience," IEEE Transactions on Energy Conversion, vol. 27, no. 1, 2012, pp. 184-195.
13. E.Z. Guerrero, A.G. Gonzáez, J.M. Lopez-Guede and I.C. Gordillo, "Simulación basada en SMA de sistemas originalmente representados con EDO," Revista Iberoamericana de Automática e Informática Industrial RIAI, vol. 8, no. 4, 2011, pp. 323-333; DOI https://doi.org/10.1016/j.riai.2011.09.011.
14. E. Simley, L.Y. Pao, R. Frehlich, B. Jonkman and N. Kelley, "Analysis of light detection and ranging wind speed measurements for wind turbine control," Wind Energy, vol. 17, no. 3, 2014, pp. 413-433; DOI 10.1002/we.1584.
15. G. Gualtieri and S. Secci, "Extrapolating wind speed time series vs. Weibull distribution to assess wind resource to the turbine hub height: A case study on coastal location in Southern Italy," Renewable Energy, vol. 62, 2014, pp. 164-176; DOI http://dx.doi.org/10.1016/j.renene.2013.07.003.
16. A. Sedaghat, A. Hassanzadeh, J. Jamali, A. Mostafaeipour and W.-H. Chen, "Determination of rated wind speed for maximum annual energy production of variable speed wind turbines," Applied Energy, vol. 205, no. Supplement C, 2017, pp. 781-789; DOI https://doi.org/10.1016/j.apenergy.2017.08.079.
17. J.G. Slootweg, S.W.H.d. Haan, H. Polinder and W.L. Kling, "General model for representing variable speed wind turbines in power system dynamics simulations," IEEE Transactions on Power Systems, vol. 18, no. 1, 2003, pp. 144-151; DOI 10.1109/TPWRS.2002.807113.
18. M. Cui, D. Ke, Y. Sun, D. Gan, J. Zhang and B.M. Hodge, "Wind Power Ramp Event Forecasting Using a Stochastic Scenario Generation Method," IEEE Transactions on Sustainable Energy, vol. 6, no. 2, 2015, pp. 422-433; DOI 10.1109/TSTE.2014.2386870.
19. M.M. Zhang, B. Tan and J.Z. Xu, "Smart load control on large-scale wind turbine blades due to extreme coherent gust with direction change," Journal of Renewable and Sustainable Energy, vol. 7, no. 2, 2015, pp. 023110; DOI 10.1063/1.4915273.
20. A. González-González, I. Etxeberria-Agiriano, E. Zulueta, F. Oterino-Echavarri and M.J. Lopez-Guede, "Pitch Based Wind Turbine Intelligent Speed Setpoint Adjustment Algorithms," Energies, vol. 7, no. 6, 2014; DOI 10.3390/en7063793.
21. E.C.C. Choi and F.A. Hidayat, "Gust factors for thunderstorm and non-thunderstorm winds," Journal of Wind Engineering and Industrial Aerodynamics, vol. 90, no. 12-15, 2002, pp. 1683-1696; DOI 10.1016/s0167-6105(02)00279-9.
22. Q. Han, F. Meng, T. Hu and F. Chu, "Non-parametric hybrid models for wind speed forecasting," Energy Conversion and Management, vol. 148, no. Supplement C, 2017, pp. 554-568; DOI https://doi.org/10.1016/j.enconman.2017.06.021.
23. F. Tagliaferri, B.P. Hayes, I.M. Viola and S.Z. Djokić, "Wind modelling with nested Markov chains," Journal of Wind Engineering and Industrial Aerodynamics, vol. 157, no. Supplement C, 2016, pp. 118-124; DOI https://doi.org/10.1016/j.jweia.2016.08.009.
24. J. Tang, A. Brouste and K.L. Tsui, "Some improvements of wind speed Markov chain modeling," Renewable Energy, vol. 81, no. Supplement C, 2015, pp. 52-56; DOI https://doi.org/10.1016/j.renene.2015.03.005.
25. Y. Wang, H. Ma, D. Wang, G. Wang, J. Wu, J. Bian and J. Liu, "A new method for wind speed forecasting based on copula theory," Environmental Research, vol. 160, 2018, pp. 365-371; DOI https://doi.org/10.1016/j.envres.2017.09.034.
26. S. Solari and M.Á. Losada, "Simulation of non-stationary wind speed and direction time series," Journal of Wind Engineering and Industrial Aerodynamics, vol. 149, no. Supplement C, 2016, pp. 48-58; DOI https://doi.org/10.1016/j.jweia.2015.11.011.
27. J. Hu, J. Wang and L. Xiao, "A hybrid approach based on the Gaussian process with t-observation model for short-term wind speed forecasts," Renewable Energy, vol. 114, no. Part B, 2017, pp. 670-685; DOI https://doi.org/10.1016/j.renene.2017.05.093.
28. R. Carapellucci and L. Giordano, "A methodology for the synthetic generation of hourly wind speed time series based on some known aggregate input data," Applied Energy, vol. 101, no. Supplement C, 2013, pp. 541-550; DOI https://doi.org/10.1016/j.apenergy.2012.06.044.
29. P.J. Schubel and R.J. Crossley, "Wind turbine blade design," Energies, vol. 5, no. 9, 2012, pp. 3425-3449.
30. L. Wang, X. Liu and A. Kolios, "State of the art in the aeroelasticity of wind turbine blades: Aeroelastic modelling," Renewable and Sustainable Energy Reviews, vol. 64, no. Supplement C, 2016, pp. 195-210; DOI https://doi.org/10.1016/j.rser.2016.06.007.
31. G. Marsh, C. Wignall, P.R. Thies, N. Barltrop, A. Incecik, V. Venugopal and L. Johanning, "Review and application of Rainflow residue processing techniques for accurate fatigue damage estimation," International Journal of Fatigue, vol. 82, no. Part 3, 2016, pp. 757-765; DOI https://doi.org/10.1016/j.ijfatigue.2015.10.007.
32. L. Vera-Tudela and M. Kühn, "Analysing wind turbine fatigue load prediction: The impact of wind farm flow conditions," Renewable Energy, vol. 107, no. Supplement C, 2017, pp. 352-360; DOI https://doi.org/10.1016/j.renene.2017.01.065.
33. R. Wagner, M. Courtney, J. Gottschall and P. Lindelöw-Marsden, "Accounting for the speed shear in wind turbine power performance measurement," Wind Energy, vol. 14, no. 8, 2011, pp. 993-1004; DOI 10.1002/we.509.
34. X. Liu, C. Lu, G. Li, A. Godbole and Y. Chen, "Effects of aerodynamic damping on the tower load of offshore horizontal axis wind turbines," Applied Energy, vol. 204, no. Supplement C, 2017, pp. 1101-1114; DOI https://doi.org/10.1016/j.apenergy.2017.05.024.
35. G. Kilic and M.S. Unluturk, "Testing of wind turbine towers using wireless sensor network and accelerometer," Renewable Energy, vol. 75, no. Supplement C, 2015, pp. 318-325; DOI https://doi.org/10.1016/j.renene.2014.10.010.
36. T. Burton, N. Jenkins, D. Sharpe and E. Bossanyi, Wind Energy Handbook, Wiley, 2011.
37. M. Gkantou, P. Martinez-Vazquez and C. Baniotopoulos, "On the structural response of a tall hybrid onshore wind turbine tower," Procedia Engineering, vol. 199, no. Supplement C, 2017, pp. 3200-3205; DOI https://doi.org/10.1016/j.proeng.2017.09.535.
38. Y. Hu, C. Baniotopoulos and J. Yang, "Effect of internal stiffening rings and wall thickness on the structural response of steel wind turbine towers," Engineering Structures, vol. 81, no. 0, 2014, pp. 148-161; DOI http://dx.doi.org/10.1016/j.engstruct.2014.09.015.
39. R. Fontecha, B. Henneke, F. Kemper and M. Feldmann, "Aerodynamic properties of Wind Turbine Towers based on Wind Tunnel Experiments," Procedia Engineering, vol. 199, no. Supplement C, 2017, pp. 3121-3126; DOI https://doi.org/10.1016/j.proeng.2017.09.557.
40. W. Liu, "Design and kinetic analysis of wind turbine blade-hub-tower coupled system," Renewable Energy, vol. 94, no. Supplement C, 2016, pp. 547-557; DOI https://doi.org/10.1016/j.renene.2016.03.068.
41. A. Smaili, A. Tahi and C. Massfon, "Thermal Analysis of Wind Turbine Nacelle Operating in Algerian Saharan Climate," Energy Procedia, vol. 18, no. Supplement C, 2012, pp. 187-196; DOI https://doi.org/10.1016/j.egypro.2012.05.030.
42. M.R. Islam, Y. Guo and J. Zhu, "A review of offshore wind turbine nacelle: Technical challenges, and research and developmental trends," Renewable and Sustainable Energy Reviews, vol. 33, no. Supplement C, 2014, pp. 161-176; DOI https://doi.org/10.1016/j.rser.2014.01.085.
43. W. Mohamed and P.-E. Austrell, "A comparative study of three onshore wind turbine foundation solutions," Computers and Geotechnics, 2017; DOI https://doi.org/10.1016/j.compgeo.2017.08.022.
44. F.P.G. Márquez, J.M.P. Pérez, A.P. Marugán and M. Papaelias, "Identification of critical components of wind turbines using FTA over the time," Renewable Energy, vol. 87, no. Part 2, 2016, pp. 869-883; DOI https://doi.org/10.1016/j.renene.2015.09.038.
45. S. Korkiakoski, E. Sarlin, R. Suihkonen and O. Saarela, "Influence of reinforcement positioning on tension-tension fatigue performance of quasi-unidirectional GFRP laminates made of stitched fabrics," Composites Part B: Engineering, vol. 112, no. Supplement C, 2017, pp. 38-48; DOI https://doi.org/10.1016/j.compositesb.2016.12.017.
46. S. Ataya and M.M.Z. Ahmed, "Damages of wind turbine blade trailing edge: Forms, location, and root causes," Engineering Failure Analysis, vol. 35, no. Supplement C, 2013, pp. 480-488; DOI https://doi.org/10.1016/j.engfailanal.2013.05.011.
47. A.C.H. Wong, T. Tian, J.K.H. Tsoi, M.F. Burrow and J.P. Matinlinna,

ACCEPTED MANUSCRIPT

"Aspects of adhesion tests on resin–glass ceramic bonding," Dental Materials, vol. 33, no. 9, 2017, pp. 1045-1055; DOI https://doi.org/10.1016/j.dental.2017.06.013.

48. A. Castorrini, A. Corsini, F. Rispoli, P. Venturini, K. Takizawa and T.E. Tezduyar, "Computational analysis of wind-turbine blade rain erosion," Computers & Fluids, vol. 141, no. Supplement C, 2016, pp. 175-183; DOI https://doi.org/10.1016/j.compfluid.2016.08.013.
49. R. Bhanushali, D. Ayre and H.Y. Nezhad, "Tensile Response of Adhesively Bonded Composite-to-composite Single-lap Joints in the Presence of Bond Deficiency," Procedia CIRP, vol. 59, no. Supplement C, 2017, pp. 139-143; DOI https://doi.org/10.1016/j.procir.2016.09.021.
50. K.M. Jespersen and L.P. Mikkelsen, "Three dimensional fatigue damage evolution in non-crimp glass fibre fabric based composites used for wind turbine blades," Composites Science and Technology, vol. 153, no. Supplement C, 2017, pp. 261-272; DOI https://doi.org/10.1016/j.compscitech.2017.10.004.
51. R.B. Rodrigues, V.M.F. Mendes, J.P.S. Catalao, S. Correia, V. Prior and M. Aguado, "An investigation over the lightning location system in Portugal for wind turbine protection development," Proc. 2008 IEEE Power and Energy Society General Meeting - Conversion and Delivery of Electrical Energy in the 21st Century, 2008, pp. 1-8.
52. Q. Zhou, C. Liu, X. Bian, K.L. Lo and D. Li, "Numerical analysis of lightning attachment to wind turbine blade," Renewable Energy, vol. 116, no. Part A, 2018, pp. 584-593; DOI https://doi.org/10.1016/j.renene.2017.09.086.
53. M. Entezami, S. Hillmansen, P. Weston and M.P. Papaelias, "Fault detection and diagnosis within a wind turbine mechanical braking system using condition monitoring," Renewable Energy, vol. 47, no. Supplement C, 2012, pp. 175-182; DOI https://doi.org/10.1016/j.renene.2012.04.031.
54. F.D. Kanellos and N.D. Hatziargyriou, "Optimal Control of Variable Speed Wind Turbines in Islanded Mode of Operation," Ieee Transactions on Energy Conversion, vol. 25, no. 4, 2010, pp. 1142-1151; DOI 10.1109/tec.2010.2048216.
55. Y. Ming, L. Gengyin, Z. Ming and Z. Chengyong, "Modeling of the wind turbine with a permanent magnet synchronous generator for integration," 2007 IEEE Power Engineering Society General Meeting, 2007, pp. 6 pp.-6 pp.
56. I.P. Girsang, J.S. Dhupia, E. Muljadi, M. Singh and L.Y. Pao, "Gearbox and Drivetrain Models to Study Dynamic Effects of Modern Wind Turbines," Ieee Transactions on Industry Applications, vol. 50, no. 6, 2014, pp. 3777-3786; DOI 10.1109/tia.2014.2321029.
57. W. Meng, Q. Yang and Y. Sun, "Adaptive control of variable-speed wind energy conversion systems with inaccurate wind speed measurement," Transactions of the Institute of Measurement and Control, vol. 37, no. 1, 2015, pp. 63-72; DOI 10.1177/0142331214531008.
58. G. Abad, J. López, M. Rodríguez, L. Marroyo and G. Iwanski, Doubly Fed Induction Machine: Modeling and Control for Wind Energy Generation, Wiley, 2011.
59. G.S. Stavrakakis and A. Sayigh, "2.10 - Electrical Parts of Wind Turbines," Comprehensive Renewable Energy, Elsevier, 2012, pp. 269-328.
60. K.A. Kragh and M.H. Hansen, "Load alleviation of wind turbines by yaw misalignment," Wind Energy, vol. 17, no. 7, 2014, pp. 971-982; DOI 10.1002/we.1612.
61. C.L. Bottasso and C.E.D. Riboldi, "Estimation of wind misalignment and vertical shear from blade loads," Renewable Energy, vol. 62, no. 0, 2014, pp. 293-302; DOI http://dx.doi.org/10.1016/j.renene.2013.07.021.
62. I.P. Girsang and J.S. Dhupia, "Pitch controller for wind turbine load mitigation through consideration of yaw misalignment," Mechatronics, vol. 32, 2015, pp. 44-58.
63. K.A. Kragh, P.A. Fleming and A.K. Scholbrock, "Increased Power Capture by Rotor Speed-Dependent Yaw Control of Wind Turbines," Journal of Solar Energy Engineering-Transactions of the Asme, vol. 135, no. 3, 2013; DOI 10.1115/1.4023971.
64. E. De Vries, "Development of two-bladed offshore wind turbine," Wind Stats Report, vol. 24, no. 2, 2011.
65. J.L. Domínguez-García, O. Gomis-Bellmunt, L. Trilla-Romero and A. Junyent-Ferré, "Indirect vector control of a squirrel cage induction generator wind turbine," Computers & Mathematics with Applications, vol. 64, no. 2, 2012, pp. 102-114; DOI https://doi.org/10.1016/j.camwa.2012.01.021.
66. K. Bedoud, A. Rhif, T. Bahi and H. Merabet, "Study of a double fed induction generator using matrix converter: Case of wind energy conversion system," International Journal of Hydrogen Energy, 2017; DOI https://doi.org/10.1016/j.ijhydene.2017.07.010.
67. N. Öztürk, A. Dalcalı, E. Çelik and S. Sakar, "Cogging torque reduction by optimal design of PM synchronous generator for wind turbines," International Journal of Hydrogen Energy, vol. 42, no. 28, 2017, pp. 17593-17600; DOI https://doi.org/10.1016/j.ijhydene.2017.02.093.
68. E. Van der Hooft, P. Schaak and T. Van Engelen, "Wind turbine control algorithms," DOWEC project-DOWEC-F1W1-EH-03-094/0, Task-3 report, 2003.
69. C. Carrillo, A.F. Obando Montaño, J. Cidrás and E. Díaz-Dorado, "Review of power curve modelling for wind turbines," Renewable and Sustainable Energy Reviews, vol. 21, no. 0, 2013, pp. 572-581; DOI http://dx.doi.org/10.1016/j.rser.2013.01.012.
70. M.H. Hansen, A.D. Hansen, T.J. Larsen, S. Øye, P. Sørensen and P. Fuglsang, Control design for a pitch-regulated, variable speed wind turbine, 2005.
71. L. Monostori and Z.J. Viharos, "Hybrid, AI- and simulation-supported optimisation of process chains and production plants," CIRP Annals, vol. 50, no. 1, 2001, pp. 353-356; DOI https://doi.org/10.1016/S0007-8506(07)62138-6.

ACCEPTED MANUSCRIPT